Mercer *et al. J Mater. Sci: Mater Eng.* (2024) 19:47
https://doi.org/10.1186/s40712-024-00195-3

Journal of Materials Science: Materials in Engineering

ORIGINAL PAPER

Open Access

Surface-activated bonding between a 3D-printed Ti-6Al-4V structure and bulk aluminum

Christopher Mercer[1*], Akira Hasegawa[2] and Naoe Hosoda[3*]

Abstract

Surface-activated bonding (SAB) of a 3D-printed Ti-6Al-4V pillar structure (fabricated by selective laser melting) to pure bulk aluminum at room temperature has been investigated. Argon beam irradiation was used to remove surface contaminants and "activate" the surfaces prior to bonding. The surface chemistry of the Ti-6Al-4V surface was analyzed using Electron Spectroscopy for Chemical Analysis (ESCA) to make sure any oxides had been removed by the irradiation procedure. The two materials were successfully bonded via SAB using special bonding apparatus, and scanning transmission electron microscopy (STEM) observation revealed a flat well-bonded interface with no obvious porosity. Furthermore, no thick reaction layer that could compromise the strength of the bond was evident. An oxide layer approximately 2 nm in thickness was observed at the interface by high-resolution TEM, but this is not considered sufficient to have a detrimental effect on bond integrity. The results of the investigation show that 3D-printed materials and structures can be successfully joined to aluminum by SAB techniques.

Keywords Surface-activated bonding; Biomimetics, 3D printing, Ti-6Al-4V

Introduction

Surface-activated bonding is an established technique of bonding two materials at room-temperature via "activation" of the material surfaces, usually by fast atom or ion bombardment prior to bonding (Suga 1990). The "activation" process generally involves the removal of surface oxides or other contaminants. The two activated surfaces are then brought together under load in a vacuum, and bonding occurs. The SAB process has been successfully demonstrated for a wide range of materials combinations, including metal–metal (Suga et al. 1992; Kim et al. 2003; Yang et al. 1997), semiconductor–semiconductor (Takagi et al. 1996; Chung et al. 1997), metal-ceramic (Suga et al. 1992), semiconductor-ceramic (Takagi et al. 1998, 1999), and metal-diamond (Fujino et al. 2015). It has also been demonstrated that SAB can be a reversible process: materials joined in this manner may be separated via heat treatment. Brittle intermetallic compounds are formed during the heat treatment process which weaken the bonded interface (Hosoda et al. 2007).

However, all previous work has involved the bonding of bulk materials. In many modern applications, the bonding of materials to certain structures or metamaterials, especially those fabricated by additive manufacturing techniques, may be desirable. But these structures and metamaterials may present challenges to successful bonding because of (i) their often inherently complex morphology and (ii) the fact that the microstructure (and hence mechanical properties) of 3D-printed materials is

*Correspondence:
Christopher Mercer
MERCER.Christopher@nims.go.jp
Naoe Hosoda
HOSODA.Naoe@nims.go.jp
[1] Additive Manufacturing Group, Research Center for Structural Materials, National Institute for Materials Science, Tsukuba, Japan
[2] Electron Microscopy Unit, Materials Fabrication and Analysis Platform, Research Network and Facility Services Division, National Institute for Materials Science, Tsukuba, Japan
[3] Smart Interface Team, Research Center for Materials Nanoarchitectonics (MANA), National Institute for Materials Science, Tsukuba, Japan

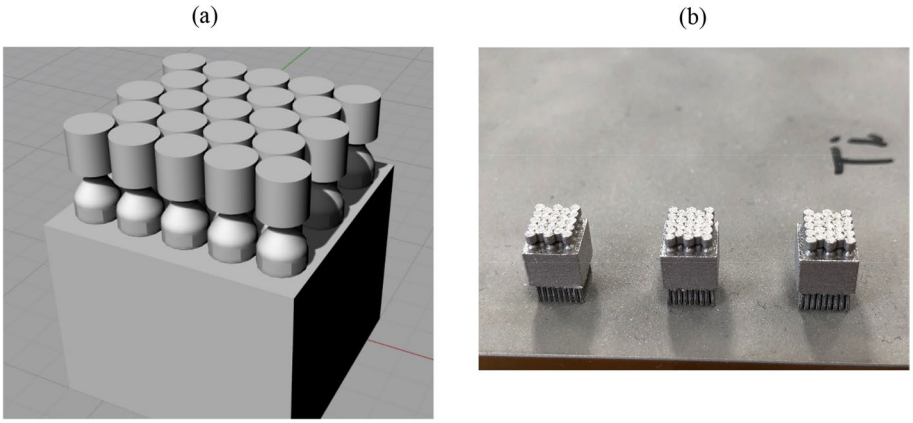

Fig. 1 Pillar structure used in the investigation. **a** CAD drawing. **b** Finished structures fabricated from Ti-6Al-4V powder

often unique and very different to that of conventionally processed materials (Bajaj et al. 2020; Neikter et al. 2018).

Therefore, the purpose of this research was to investigate the ability of the SAB technique to bond bulk aluminum to a 3D-printed structure fabricated from Ti-6Al-4V powder. The structure consisted of an arrangement of upright, cylindrical pillars designed to approximately simulate the type of structure found on the underside of many insect feet (Gorb et al. 2007; Heepe and Gorb 2014). Structures of this type are of considerable interest in the field of biomimetics. Dissimilar materials were chosen to make the study challenging and meaningful, and Ti-6Al-4V was selected since it is a well-known aerospace alloy, widely used in many advanced engineering applications. However, any material that can be successfully fabricated via 3D printing could, in principle, be substituted. Possibilities include stainless steel or other ferrous alloys, nickel-based alloys, or refractory metals such a tungsten and molybdenum. However, the nature of the bonding would be expected to change with different material/microstructure combinations. In this case, successful bonding of the bulk aluminum to the 3D-printed structure is demonstrated, and the nature and composition of the bond interface is examined via electron microscopy and quantitative analysis techniques.

Experimental procedure

Preparation of Ti-6Al-4V pillar structure and aluminum

The structure chosen for 3D printing is shown in Fig. 1. It consists of an array of pillar-like features attached to a nearly cubic base. This structure was chosen because it is a good example of the type of structure of interest in bonding applications such as SAB, since it approximately resembles the morphology of the adhesion elements (setae) found on the legs of beetles and other similar insects (Gorb et al. 2007; Heepe and Gorb 2014). A drawing of the structure was first created using the computer-aided design (CAD) software Rhinoceros (Robert McNeel & Associates, Seattle, WA, USA). Several pillar structures were then fabricated from CL 41TI ELI (Ti-6Al-4V) powder (GE Additive, Cincinnati, OH, USA) simultaneously via selective laser melting using a Concept Laser Mlab cusing R 3D laser printer (GE Additive, Cincinnati, OH, USA). The chemical composition of the powder is given in Table 1. The machine parameters employed during the 3D printing are summarized in Table 2. The dimensions of each printed structure were 6 mm × 6 mm × 7 mm (in height).

Table 1 Chemical composition of Ti-6Al-4V powder

Element	Wt%
Titanium	Balance
Aluminum	5.5–6.5
Vanadium	3.5–4.5
Iron	0–0.25
Carbon	0–0.08
Oxygen	0–0.13
Nitrogen	0–0.05
Hydrogen	0–0.012

Table 2 Laser printing parameters

Parameter	Value
Laser power	95 W
Laser movement speed	900 mm/s
Spot size	30 µm
Slice thickness	25 µm

Following 3D printing, the flat top surfaces of the pillars comprising the structure were metallographically prepared by firstly grinding with silicon carbide paper followed by diamond polishing (9 μm, 3 μm, and 1 μm). Finally, colloidal silica was used to produce a mirror finish. The aluminum sample comprised a 3-mm-diameter cylinder of high-purity aluminum possessing one hemispherical surface with a radius of curvature of 25 mm. This curved surface was also initially ground using silicon carbide paper and then polished to a mirror finish with alumina powder. Then, the Al samples were annealed at 120 °C in an argon atmosphere for 2 h, before being electrochemically polished using a solution of 30% perchloric acid and 70% ethanol.

Surface-activated bonding procedure

Following polishing, the samples were transferred to the SAB bonding apparatus. Such apparatus has been described in detail elsewhere (Fujino et al. 2015) but basically includes a process chamber and a bonding chamber held under vacuum. In the process chamber, the samples were subjected to high-speed argon atomic beam irradiation (1.0 kV, 20 mA). The duration of the Ar beam irradiation was 30 min and 7 min for the Ti-6Al-4V and pure Al, respectively. The optimum parameters for the irradiation process were established in a previous investigation (Hosoda et al. 1998). Less time was needed for the aluminum because this material had been electrochemically polished prior to the irradiation. The purpose of the irradiation was to remove contaminants from the sample surfaces to be bonded and produce active surfaces. Electron Spectroscopy for Chemical Analysis (ESCA) (ULVAC-PHY Model 1600, ULVAC-PHY, Inc., Chigasaki, Japan) was performed in the analysis chamber of the bonding apparatus on the polished Ti-6Al-4V surface before and after irradiation. The samples were then transferred to the bonding chamber via the transfer chamber. Inside the bonding chamber, the Ti-6Al-4V and pure Al surfaces were brought into contact and bonded at room temperature under a 140 N load applied for 1 min (Fig. 2a). Following loading, the sample was raised within the bonding chamber to ensure that the two materials were successfully joined (Fig. 2b).

Testing and analysis methods

The strength of the bond between the Ti-6Al-4V and the Al was determined via a tensile test in which one of the bonded Ti-6Al-4V/Al samples was pulled apart using a servo-electric tensile testing machine (LTS-1kNB, MinebeaMitsumi Inc., Tokyo, Japan) using a digital force gauge with a 1 kN capacity (LTTU, MinebeaMitsumi Inc., Tokyo, Japan) under displacement control at a displacement rate of 5 mm/min. The load required for separation was measured and the corresponding failure stress of the bond was determined.

Thin foils were taken from another of the samples for analysis of the bonded interface by scanning transmission electron microscopy (STEM) (JEM-2100F, JEOL, Tokyo, Japan) and high-resolution transmission electron microscopy (HR-TEM) (JEM-2100F, JEOL, Tokyo, Japan). The thin foils were prepared by initial sectioning with a diamond saw followed by diamond polishing of

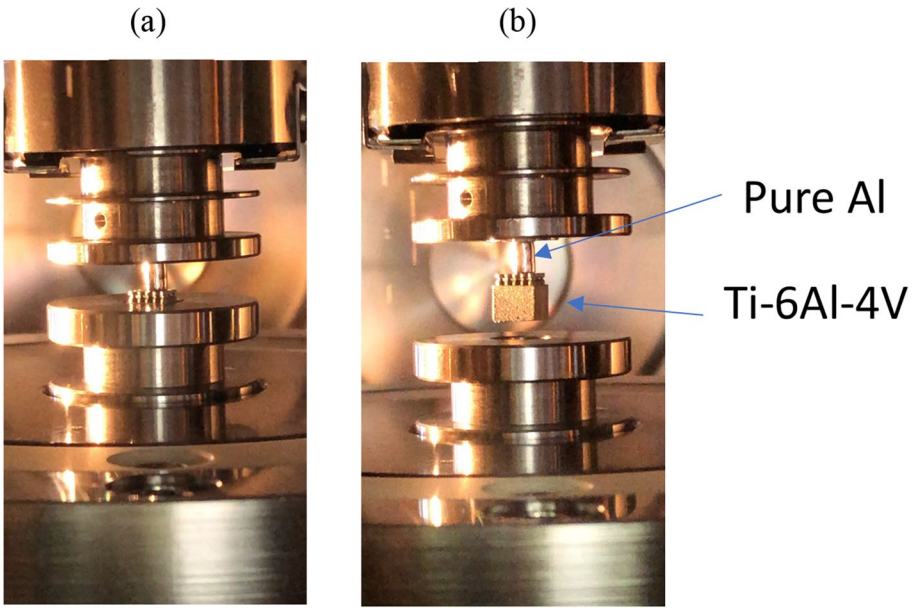

Fig. 2 Surface-activated bonding process. **a** Sample under load. **b** Successfully bonded Ti-6Al-4V structure and pure aluminum cylinder

the bonded interface. Finally, the polished surface featuring the bonded interface was shaped using a focused ion beam (FIB) (Helios Nanolab 600i, Thermo Fisher Scientific, Waltham, MA, USA) technique. Energy-dispersive spectroscopy (EDS) analysis and element mapping (EX-24200M1G2T, JEOL, Tokyo, Japan) were also performed during the STEM observation.

Results and discussion

Electron Spectroscopy for Chemical Analysis (ESCA) spectra taken from the Ti-6Al-4V surface before and after irradiation are presented in Fig. 3. Prior to Ar-atom irradiation, the presence of metal oxide is evident on the polished Ti-6Al-4V surface. Carbon and silicon were also detected. Silicon is considered an impurity adhering to the Ti-6Al-4V surface. No Al or V were detected by ESCA. However, following irradiation, the quantity of

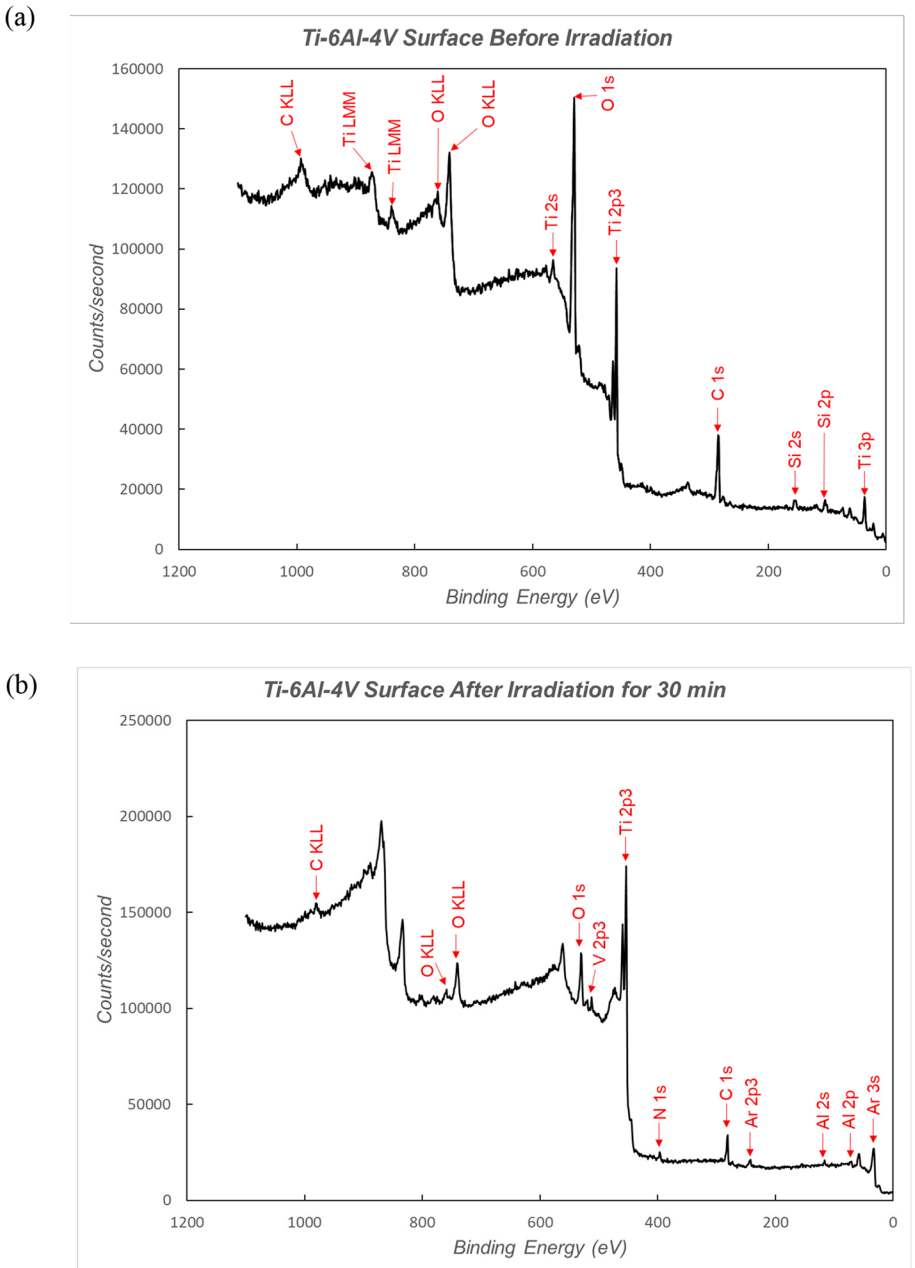

Fig. 3 Electron Spectroscopy for Chemical Analysis (ESCA) spectra taken from the Ti-6Al-4V surface. **a** Before irradiation. **b** After irradiation

oxygen decreases significantly. Also, small amounts of Al and V were detected following irradiation. These results indicate that a 30-min duration of Ar irradiation was sufficient to remove oxide and other contaminants and produce a clean, active metal surface.

The fracture surface of the bonded sample subjected to tensile testing is shown in Fig. 4. It is evident from Fig. 4 that most of the failure occurred at the aluminum interface in areas that were not successfully bonded. A moderately low bond failure strength of 9.2 MPa (117 N force) was measured. However, it is considered that this low value is due to the fact areas of the sample were not properly bonded and not due to a low bond strength in the successfully bonded areas. However, it should be noted that the bond strength will typically be lower in the case of such 3D-printed structures compared with solid, conventional materials. This is due to the more complex geometry and the frequent existence of gaps or spaces in the 3D structure. The principal reason for the incomplete bonding is thought to be due to different rates of chemical polishing and argon beam sputtering in the polycrystalline aluminum. Different grain orientations will be subject to different polishing and sputtering rates. This will produce small steps on the metal surface, and consequently, small gaps will exist between the two bonded materials.

A dark-field STEM image of the bonded interface between the Ti-6Al-4V and the pure Al is shown in Fig. 5. It can be seen from the image that a high-integrity bond with no discernible porosity has been achieved by the SAB process. In addition, there is no indication of the presence of a thick reaction layer at the interface. These are good results and confirm that a 3D-printed titanium structure can be successfully bonded by SAB to pure aluminum. High-resolution TEM imaging (Fig. 6) revealed the presence of a very thin (~2 nm) amorphous layer at the bonded interface. Since the interface layer is extremely thin, it is not considered that it would have a significant effect on bond integrity. Furthermore, such layers generally exhibit good chemical stability. In fact, past experience has indicated that the strength of such bonds tends to increase over time (Matsusaka et al. 1999).

It is possible, in principle, to reduce the thickness of the interface reaction layer even further. Since the layer

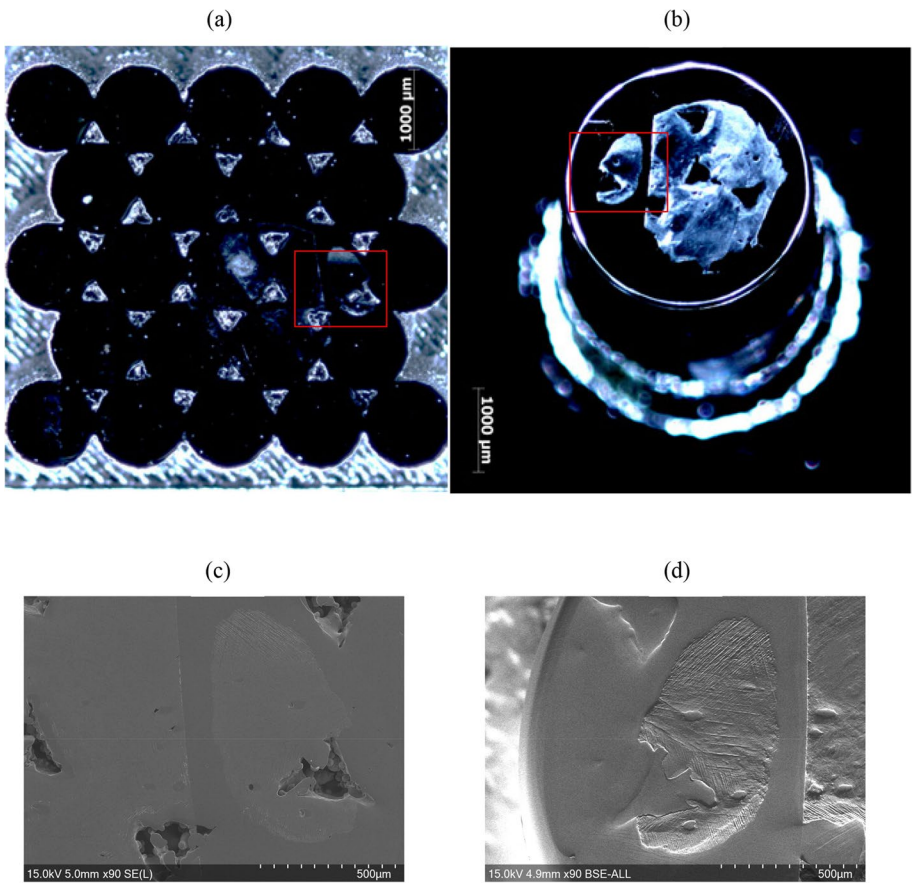

Fig. 4 Fracture surface of bonded sample following separation via tensile test. **a** Optical micrographs of whole sample. **b** Optical micrograph of individual pillar. **c** Scanning electron micrograph of region highlighted in **a**. **d** Scanning electron micrograph of region highlighted in **b**

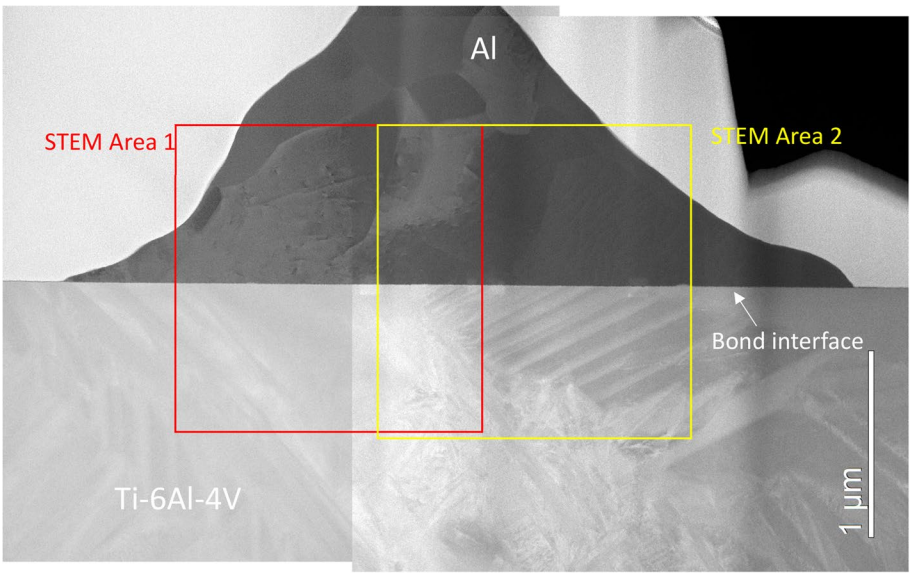

Fig. 5 Dark-field STEM image of bonded interface between Ti-6Al-4V and Al

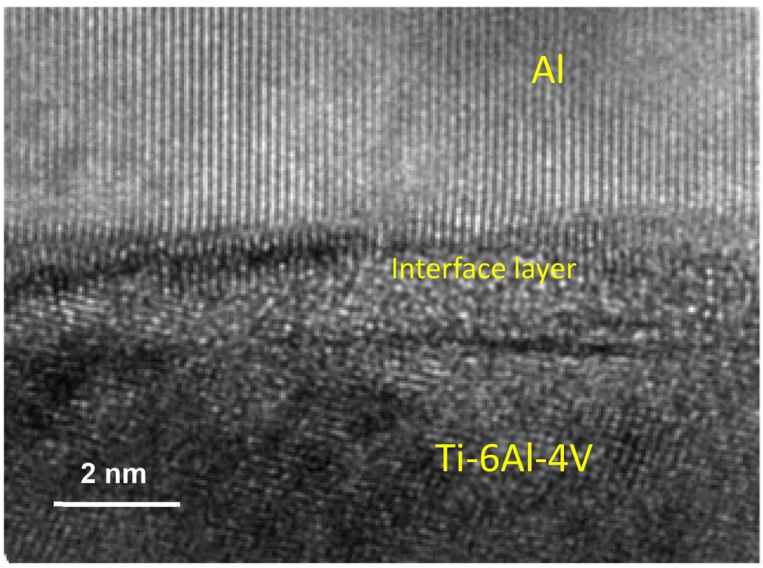

Fig. 6 High-resolution TEM image of bonded interface between Ti-6Al-4V and Al

is composed of oxide, any attempts to reduce oxygen levels at any stage of the 3D printing/SAB bonding process should result in a thinner interface layer. The three primary sources of oxygen are (i) as an impurity in the Ti-6Al-4V powder, (ii) residual O_2 gas in the argon atmosphere of the 3D printing chamber, and (iii) trace amounts of gases such as O_2, CO_2, and H_2O in the vacuum chamber of the SAB apparatus. Additionally, minimizing exposure time of the clean, active metal surface to the gases in the vacuum chamber prior to bonding should further decrease the amount of oxygen adsorbed onto the metal surface.

Energy-dispersive spectroscopy (EDS) analysis of the interface region is presented in Fig. 7. The oxygen profile exhibits a peak right in the interface region (Fig. 7a), indicating that the thin amorphous layer is composed of oxide. It is surmised that the oxide is either aluminum or titanium oxide or a mixture of these oxides. An EDS element map of the interface region is shown in Fig. 7b. The existence of an interfacial oxide layer can be clearly

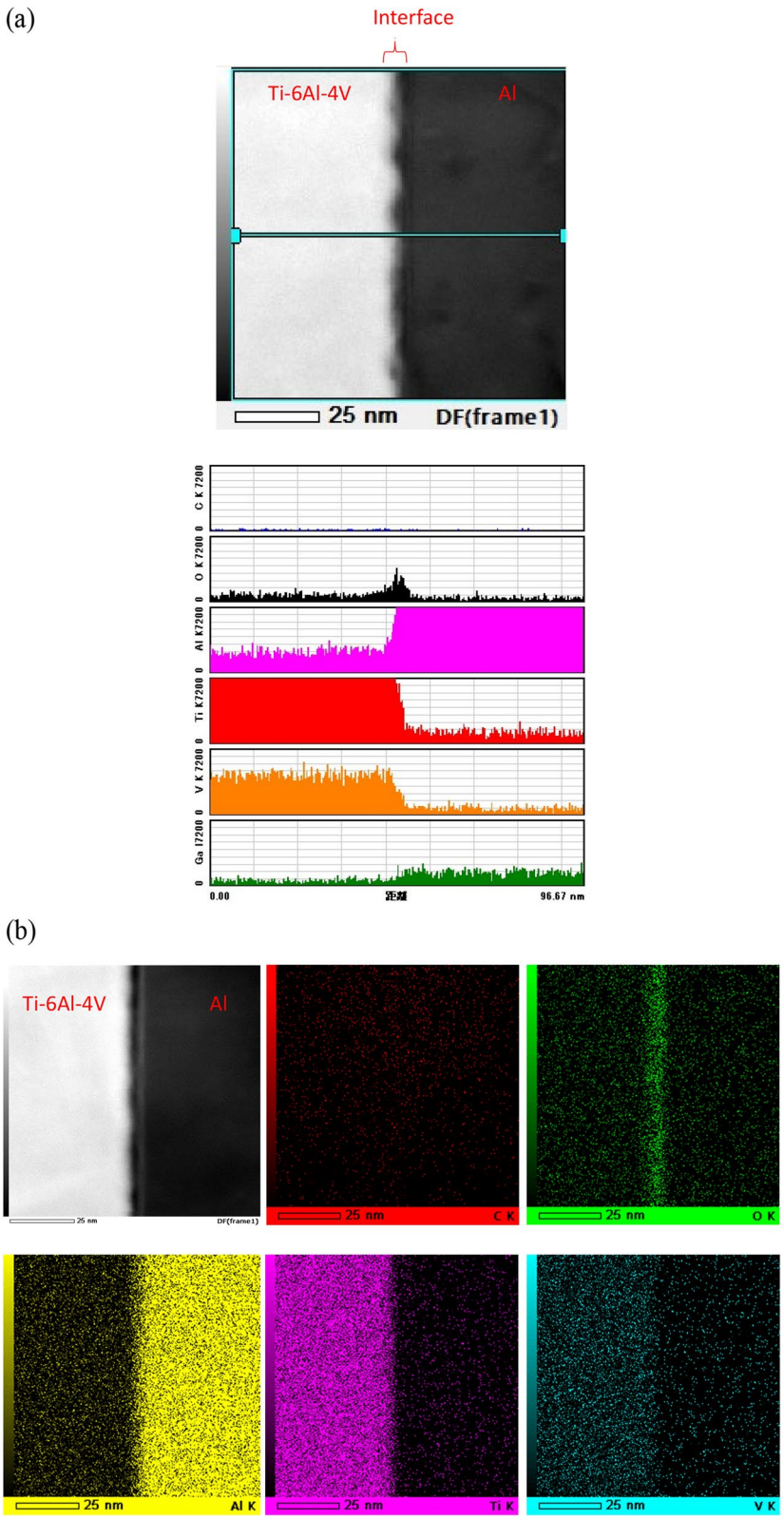

Fig. 7 Energy-dispersive spectroscopy analysis of bond interface region. **a** Line distribution profile (from STEM Area 1 in Fig. 5). **b** Two-dimensional element map (from STEM Area 2 in Fig. 5)

deduced from the oxygen distribution across the bond interface.

Surface-activated bonding can be a superior method of joining materials when compared to other bonding techniques. For example, diffusion bonding often results in the formation of thick, brittle reaction layers. Furthermore, the SAB process is particularly well suited to the bonding of 3D-printed structures like the one presented in this study. Bonding methods such as friction welding are not suitable for this application, since they could lead to fracture of the slender pillars that comprise the structure.

Concluding remarks

In this study, a 3D-printed pillar structure fabricated from Ti-6Al-4V powder using selective laser melting has been successfully joined via surface-activated bonding at room temperature to pure aluminum. A high-integrity bond with no discernable porosity was produced. In addition, no thick reaction layer was formed at the bond interface, only a very thin (~2 nm) amorphous oxide layer. Thick reaction layers can often compromise bond integrity. The investigation has demonstrated that 3D-printed metallic structures, despite their often complex shapes and unconventional microstructures, can be effectively joined to other materials using SAB techniques. Such bonding could prove especially useful when, for example, attaching biomimetic structures (such as those based on the adhesive setae found on an insect tarsus) to appropriate metallic substrates. For instance, in the field of robotics, SAB could be used to attach 3D-printed biomimetic limb structures (e.g., feet, legs, wings) to some kind of body or base. In addition, SAB is particularly well suited to the bonding of electronic components and the manufacture of micro-chips in the semiconductor industry.

Acknowledgements
The authors thank Mr. Koji Nakazato at the National Institute for Materials Science, Tsukuba, Japan, and Ms. Tae Tawara at the University of Tsukuba, Tsukuba, Japan, for their technical support.

Authors' contributions
Conceptualization, N.H.; design, N.H. and C.M.; investigation, N.H. and A.H.; writing—original draft preparation, N.H. and C.M.; writing—review and editing, N.H. and C.M.; funding acquisition, N.H. All authors have read and agreed to the published version of the manuscript.

Funding
Part of this work was supported by the "Nanotechnology Platform" of the Ministry of Education, Culture, Sports, Science and Technology (MEXT), Grant Number F-21-BA-0025.

Data availability
The datasets presented in this article are not readily available because they are proprietary.

Declarations

Competing interests
The authors declare no competing interests.

Received: 21 August 2024 Accepted: 27 November 2024
Published online: 20 December 2024

References

Bajaj P, Hariharan A, Kini A, Kürnsteiner P, Raabe D, Jägl EA (2020) Steels in additive manufacturing: A review of their microstructure and properties. Mater Sci Eng, A 772:138633
Chung TR, Yang L, Hosoda N, Takagi H, Suga T (1997) Wafer direct bonding of compound semiconductor silicon at room temperature by the surface activated bonding method. Appl Surface Sci 117–118:808–812
Fujino M, Hosoda N, Suga T, Ishikawa N, Kuwayama N (2015) Surface activated bonding between bulk single crystal diamond and bulk aluminum. Japanese J Appl Phys 54:081301
Gorb S, Varenberg M, Peressadko A, Tuma J (2007) Biomimetic mushroom-shaped fibrillar adhesive microstructure. J R Soc Interface 4:271–275
Heepe L, Gorb SN (2014) Biologically inspired mushroom-shaped adhesive microstructures. Annu Rev Mater Res 44:173–203
Hosoda N, Kyogoku Y, Suga T (1998) Effect of the surface treatment on the room-temperature bonding of Al to Si and SiO_2. J Mater Sci 33:253–258
Hosoda N, Suga T, Obara S, Imagawa K (2007) UHV-bonding and reversible interconnection. Trans Japan Soc Aero Space Sci 49:197–202
Kim TH, Howlader MMR, Itoh T, Suga T (2003) Room temperature Cu–Cu direct bonding using surface activated bonding method. J Vac Sci Technol A 21:449–453
Matsusaka S, Takahashi Y, Inoue K (1999) Study on the time dependence of bond strength in room temperature bonding. Quarterly J Japan Welding Soc 17:583–588
Neikter M, Åkerfeldt P, Pederson R, Antti M-L, Sandell V (2018) Microstructural characterization and comparison of Ti-6Al-4V manufactured with different additive manufacturing processes. Mater Charact 143:68–75
Suga T (1990) Room temperature bonding. Bull Japan Inst Metals 29:944–947
Suga T, Takahashi Y, Takagi H, Gibbesch B, Elssner G (1992) Structure of Al-Al and Al-Si_3N_4 interfaces bonded at room temperature by means of the surface activated bonding method. Acta Metall Mater 40(Suppl):133–137
Takagi H, Kikuchi K, Maeda R, Chung TR, Suga T (1996) Surface activated bonding of silicon wafers at room temperature. Appl Phys Lett 68:2222–2224
Takagi H, Maeda R, Chung TR, Suga T (1998) Low-temperature direct bonding of silicon and silicon dioxide by the surface activation method. Sens Actuators A 70:164–170
Takagi H, Maeda R, Hosoda N, Suga T (1999) Room-temperature bonding of lithium niobate and silicon wafers by argon-beam surface activation. Appl Phys Lett 74:2387–2389
Yang L, Hosoda N, Suga T (1997) Investigations on the interface microstructure of stainless steel/aluminum joints created by the surface activated bonding method. Interface Sci 5:279–286

Publisher's Note